Pascual-Jose, B.; Del Río, C.; Mosa, J.; Ribes-Greus, A. (2023). Dielectric properties OF 40SiO(2)-40P(2)O(5)-20ZrO(2) /sulfonated styrene-ethylene-butylene-styrene hybrid membranes for proton exchange membrane fuel cells. Polymer. 271. https://doi.org/10.1016/j.polymer.2023.125814

DIELECTRIC PROPERTIES OF $40SiO_2$-$40P_2O_5$-$20ZrO_2$ /SULFONATED STYRENE-ETHYLENE-BUTYLENE-STYRENE HYBRID MEMBRANES FOR PROTON EXCHANGE MEMBRANE FUEL CELLS.

B. Pascual-Jose[1], C. del Río[2], J. Mosa[3], A. Ribes-Greus[1,*]

[1] Institute of Technology of Materials (ITM), Universitat Politècnica de València (UPV), Camí de Vera, s/n, 46022, Spain.

[2] Institute of Polymer Science and Technology (ICTP-CSIC), Juan de la Cierva 3, 28006 Madrid, Spain.

[3] Institute of Ceramics and Glass (ICV-CSIC), Kelsen 5, 28049 Madrid, Spain.

[*]**Corresponding author: A. Ribes-Greus** aribes@ter.upv.es

Abstract

The dielectric spectra of a series of hybrid membranes prepared with sulfonated styrene-ethylene-butylene-styrene (sSEBS), as the polymeric matrix, and zirconia modified phosphosilicate ($40SiO_2$-$40P_2O_5$-$20ZrO_2$), as inorganic filler through direct infiltration, was analysed. All the membranes displayed characteristic sSEBS spectra, consisting of three molecular relaxations: A non-cooperative (β) relaxation and two cooperatives (α_{EB}, α_{PS}) ones ascribed to the glass transition of the ethylene-butylene and the polystyrene blocks, respectively. As a result of the infiltration of the inorganic component ($40SiO_2$-$40P_2O_5$-$20ZrO_2$), the dielectric spectra were considerably modified. Accordingly, the formation of a dynamic crosslinking (M-O-M' bonds, with M = P, Si, Zr) difficulties the motion of the α_{EB} process, thus shifting it towards higher temperatures. Moreover, a significant plasticisation effect was found at high temperatures, which facilitates the activation of the α_{PS} process. Furthermore, the decreasing values of the fragility parameter, due to the infiltration of the inorganic filler, revealed that all hybrid membranes displayed an arrangement of molecular chains and a strong behaviour. Thus, higher resistance to sudden temperature changes is expected. The optimum infiltration time is between 10 and 20 minutes since it provides acceptable values of electric permittivity, and the induced dynamic crosslinking brings the glass transitions of both blocks closer. Consequently, a complete characterisation of the molecular mobility by studying the spectrum of dielectric relaxations enables to fine-tune the membranes for an optimum design focused on its application in a proton exchange membrane fuel cell (PEMFC).

Keywords

PEMFC, dielectric properties, sulfonated SEBS.

Highlights

- Crosslinking restricts molecular motions in sSEBS-Zr membranes at low temperatures.
- Plasticisation eases molecular motions in sSEBS-Zr membranes at low temperatures.
- The inorganic network closes the gap between cooperative molecular processes.
- sSEBS-Zr hybrid membranes display lower fragility values than sSEBS ones.

Graphical Abstract

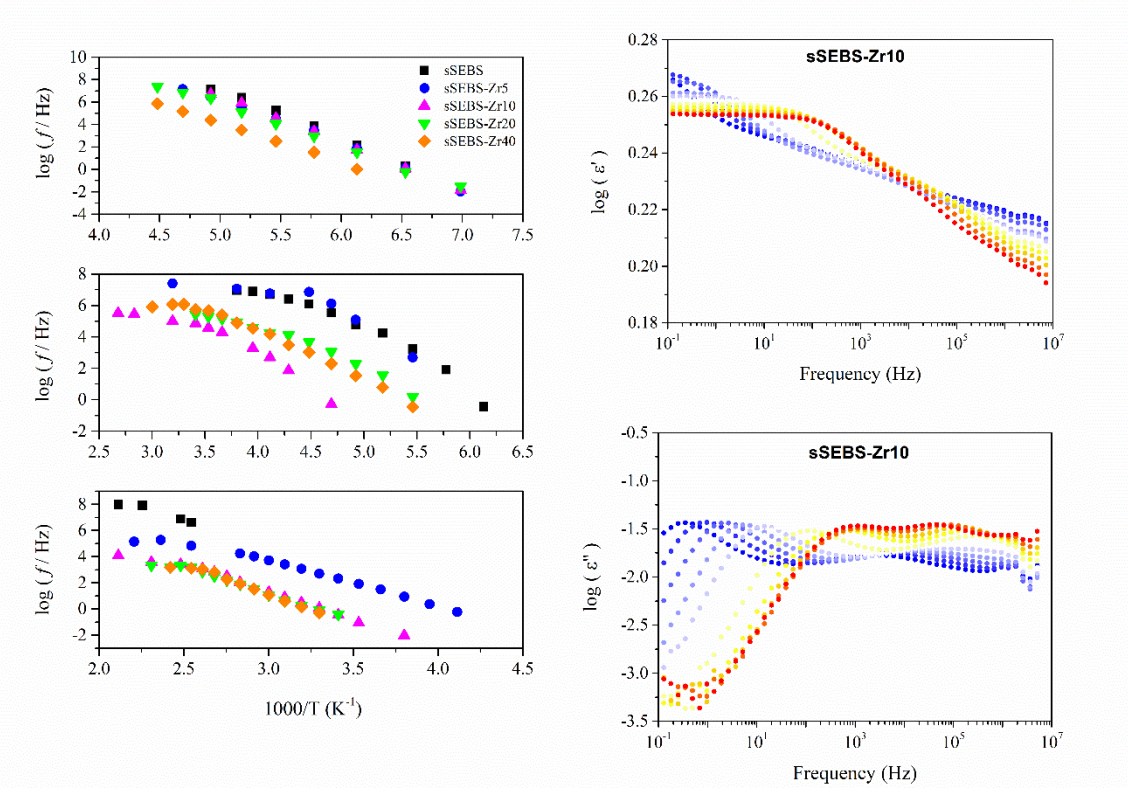

1. Introduction

Block copolymers are desirable as polymer electrolytes for fuel cell applications due to their complex morphology, allowing the development of hydrophilic and hydrophobic domains in the same microstructure [1–3]. Accordingly, SEBS is a thermoplastic elastomer with desirable properties such as excellent heat, UV and weathering resistance or low electric conductivity. However, its major drawback compared to Nafion is its low proton conductive capacity. For that reason, sulfonation of SEBS membranes has been proposed since it displays a modified microstructure to achieve good proton conductivity [4–7]. Nonetheless, although an increment in its proton conductive capacity was found, results showed that many sulfonic groups caused high water uptake levels and, therefore, swelling-related problems [8]. A more holistic approach is needed to solve these issues, and subsequently, an inorganic filler is used. The filler would enhance the chemical, mechanical and thermal stability [7,9,10]. Many fillers have been successfully employed, such as silica, alumina or titania, although it might diminish its conductive capacity [11–18].

The hybrid membranes studied were synthesised via sol-gel processing by direct infiltration of the inorganic component ($40SiO_2$-$40P_2O_5$-$20ZrO_2$). The main feature of this technique is that it generates an interpenetrating network preferentially into the ionic phase of the copolymer, enhancing its compatibility.

In a previous paper written by the same authors [6], the dielectric spectra of neat SEBS and sulfonated sSEBS show two apparent cooperative motions corresponding to each block's glass transition. Due to the different nature of each block, there is a large temperature gap between them. However, the infiltration of the inorganic precursor has been observed to create another relaxation process whose origin is the motion of the generated network. Nonetheless, this is not always the case and depends on the inorganic concentration, which is directly related to the infiltration time. Thus, determining the molecular structure of the hybrid membrane is of great importance in understanding how parameters such as the concentration of the inorganic precursor or the synthesis route are beneficial for its applicability as polymer electrolytes for fuel cell applications [5,13,19–26].

In Stenina et al. [27], the features affecting the overall performance of several ion-exchange membranes in transfer processes are reviewed. Among them, selectivity of the transport processes and ionic conductivity are regarded as the most important, determined by ionic and molecular mobility. Accordingly, dielectric thermal analysis (DETA) is a useful technique to provide information on the molecular structure of the membranes and on the proton conductivity, provided that it depends on molecular mobility [28]. Indeed, there are two types of transport mechanisms: vehicular and proton hopping (or Grotthuss mechanism). In the former, the proton is carried by a vehicular entity, such as a particular molecule. Contrarily, the latter transfers the proton through a hydrogen bond network, which is also considered more efficient since it does not require high levels of mobility [29]. Both mechanisms are correlated with the macromolecular origin of the molecular motion that is either coupled or uncoupled. Subsequently, an Arrhenius model or a Vogel-Fulcher-Tamman-Hesse (VFTH) model is related to a Grotthuss or vehicular mechanism of proton conductivity, respectively [29]. Therefore, a detailed analysis of the molecular mobility is of paramount importance for the optimum design of polyelectrolytes for proton exchange membrane fuel cell (PEMFC) applications.

Therefore, this paper characterises the dielectric spectra of a set of hybrid infiltrated membranes sSEBS-Zr, in conjunction with neat and sulfonated SEBS to determine the variations induced by the infiltration process. The analysis of the resultant dielectric spectra is expected to provide information on the molecular structure of the membranes. Furthermore, the study of the temperature dependence of the molecular relaxations is performed to obtain information on the thermal stability of the hybrid membranes. Consequently, the dielectric spectra and all their derived parameters are analysed to determine whether incorporating the inorganic network provides sufficient improvements at a molecular level to consider any of these membranes suitable for fuel cell applications.

2. Experimental procedure and calculations

2.1 Materials and preparation of hybrid membranes

The preparation of the hybrid membranes was conducted as described elsewhere [8]. Briefly, the hybrid polymer membranes based on styrene-ethylene-butylene-styrene triblock copolymer (SEBS) were prepared from SEBS (Dynasol, Calprene CH-6120) containing 32 wt% of styrene units. The membranes were cast from chloroform solutions

employing Doctor Blade technique (BYK Instruments). Regarding the sulfonation, the process was performed by immersing the membranes in a trimethylsilyl chlorosulfonic (Sigma-Aldrich) solution in 1,2-dichloroethane (DCE, Scharlau) with a molar concentration of 0.3 for 2 hours. Concerning the infiltration process, sulfonated SEBS membranes were swelled in H_2SO_4 1N at 80ºC for 2 hours and then immersed in the $40SiO_2$-$40P_2O_5$-$20ZrO_2$ sol solution at 80ºC for 5, 10, 20 and 40 minutes, respectively. Then they were thermally treated to perform the inorganic polycondensation reaction at 50 ºC for 1 hour and 120 ºC for 2 hours. Finally, the membranes were cleaned with ethanol at 80 ºC for 2 hours for the last process step. Afterwards, the membranes were dried for another hour at the same temperature.

The labelling of neat and sulfonated and the hybrid styrene ethylene butylene styrene membranes are labelled as SEBS and sSEBS, respectively. The hybrid membranes were labelled according to the infiltration time are referred to as sSEBS-Zr5, sSEBS-Zr10, sSEBS-Zr20 and sSEBS-Zr40.

2.2 Dielectric Thermal Analysis assessment

The impedance measurements were conducted using a Novocontrol Broadband Dielectric Impedance Spectrometer (BDIS), connected to a Novocontrol Alfa-A Frequency Response Analyzer. All the measurements were obtained under isothermal conditions by increasing in steps of 10 K. The sample electrode assembly (SEA) consisted of two stainless steel electrodes filled with the sample. Eventually, to avoid interference in the measurements caused by electrode polarisation, a thin PTFE film was inserted as a blocking layer between the sample and one electrode. Consequently, the resulting SEA was directly placed in the cell.

The dielectric spectra were analysed in terms of the complex permittivity (ε^*) using as many Havriliak-Negami (HN) functions as needed [30–32]. All the characteristic parameters of each relaxation process were determined as shown in **Eq.1**:

$$\varepsilon^*(w) - \varepsilon_\infty = \sum_k \mathrm{Im}\left[\frac{\Delta\varepsilon}{\left\{1 + (iw\tau_{HNk})^{a_k}\right\}^{b_k}}\right] \qquad \textit{(Eq.1)}$$

Where:

147 τ_{HN} is the Havriliak-Negami relaxation time. Thus, the sub-index *k* represents the number
148 of individual HN contributions. (*a* and *b)* are parameters corresponding to the width and
149 asymmetry of the relaxation peak. $\Delta\varepsilon$ is the value of the relaxation strength.

150 The analysis of the temperature dependence of the relaxation times is performed in terms
151 of an Arrhenius equation (**Eq. 2**) if the motion is non-cooperative or through a Vogel-
152 Fulcher-Tamman-Hesse (VFTH) equation (**Eq. 3**) if the relaxation is of cooperative
153 origin. The fragility parameter (**Eq. 4**) is calculated to determine whether the structure is
154 thermally stable or unstable [27–40].

155 $$f_{max} = f_0 \exp\left(\frac{-E_a}{R\,T}\right) \quad (Eq.2)$$

156

157 $$\tau\,(T) = \tau_0 \exp\left(\frac{B}{T - T_{VFTH}}\right), T_{VFTH} < T_g \quad (Eq.3)$$

158

159 $$m = \frac{B\,T_g}{ln(10)\left(T_g - T_{VFTH}\right)^2} \quad (Eq.4)$$

160 Where: f_{max} refers to the maximum frequency; τ is the relaxation time, f_0 and τ_0 are pre-
161 exponential terms, *B* is an activation parameter, T_{VFTH} is the temperature obtained from
162 the best fit of the VFTH equation, T_g is the glass transition temperature, E_a is the
163 activation energy, and *R* is the ideal gas constant.

164

165 **3. Results and Discussion**

166 The analysis of the dielectric spectra is performed through the complex permittivity
167 formalism (ε*). The frequency and temperature dependence of its real (ε') and imaginary
168 (ε'') parts are studied in the frequency range $f = 10^{-1} – 10^7$ Hz from 123 K to 473 K. The
169 dielectric spectra of all the studied membranes consist of several relaxation processes
170 [6,44]. Consequently, a molecular motion labelled as β was observed at low temperatures.
171 Additionally, due to SEBS microphase separated morphology, the membrane's spectra
172 display several relaxations corresponding to the poly (ethylene-butylene) (PEB) and
173 polystyrene (PS) blocks that were labelled as α_{EB} and α_{PS}, correspondingly. The two α
174 relaxations are ascribed to the glass transition of both blocks. Moreover, interfacial
175 polarisation and conductivity were observed at high temperatures overlapping the

relaxation spectra. This phenomenon, however, is not included in the analysis as it is out of the scope of this work.

The isothermal values of ε' for a range of selected temperatures are presented in **Figure 1** for all the membranes. Neat SEBS is a nonpolar thermoplastic elastomer, and these features are reflected in the spectrum. The real isothermal permittivity ε' is a nearly continuous line at each temperature. Only at high temperatures have a small shoulder corresponding to the PS block's glass transition [6]. The spectrum of sSEBS behaves similarly, the main difference being that now the values of ε' are higher due to the presence of the sulfonic groups [6,44]. Thus, both spectra are characterised by significant differences in the molecular motions of the PEB and PS blocks. However, the spectra of the hybrid infiltrated membranes sSEBS-Zr display significant variations concerning sSEBS. Indeed, a shift towards lower frequencies is observed, which extends as the infiltration time (t_{inf}) in the $40SiO_2$-$40P_2O_5$-$20ZrO_2$ solution increases. This is evidence that the formation of the inorganic phase inside sSEBS has a plasticising effect. Another observable consequence of adding the $40SiO_2$-$40P_2O_5$-$20ZrO_2$ inorganic filler is a significant drop in the values of ε' when the infiltration time increases.

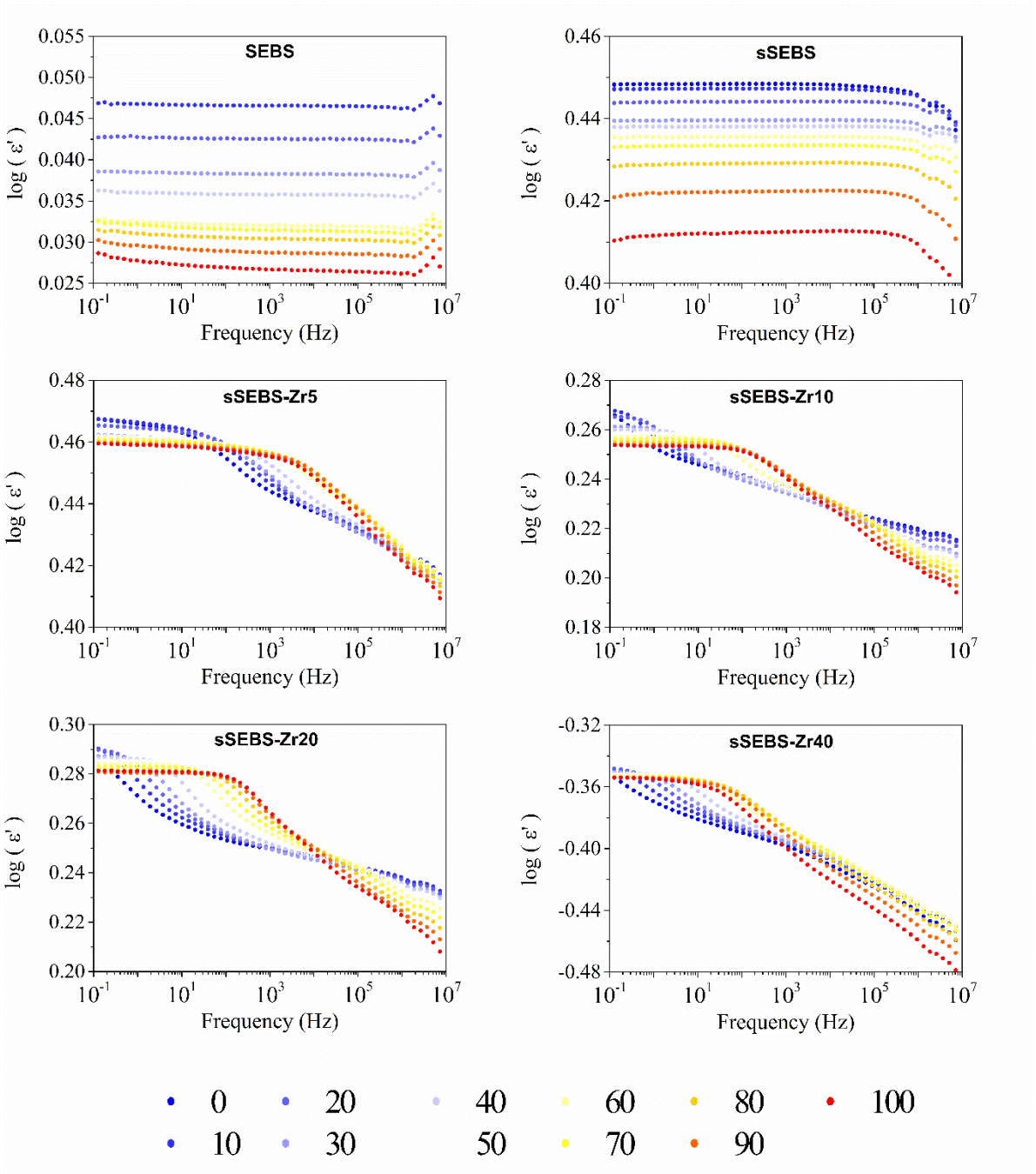

Figure 1. Logarithm of the real component of the complex permittivity for the styrene-ethylene-butylene-styrene (SEBS), sulfonated SEBS (sSEBS) and all hybrid SEBS (sSEBS-Zr5, sSEBS-Zr10, sSEBS-Zr20 and sSEBS-Zr40).

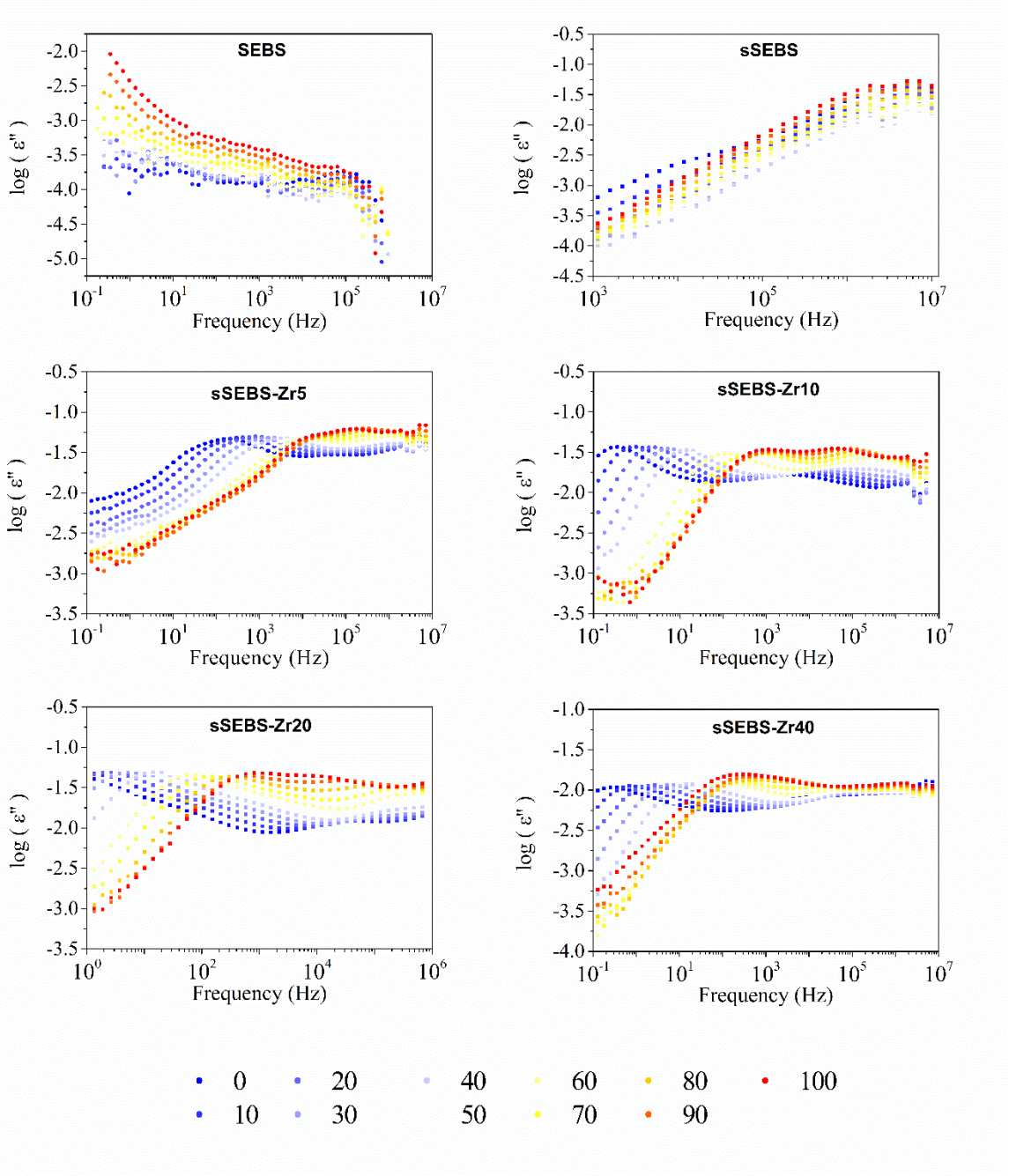

Figure 2. Logarithm of the imaginary component of the complex permittivity for the styrene-ethylene-butylene-styrene (SEBS), sulfonated SEBS (sSEBS) and all hybrid SEBS (sSEBS-Zr5, sSEBS-Zr10, sSEBS-Zr20 and sSEBS-Zr40).

Figure 2 shows the imaginary part of the dielectric permittivity ε'' shift towards lower frequencies of the molecular relaxations in the hybrid membranes sSEBS-Zr plotted in terms of the complex part. The decrease in ε' values, observed in **Figure 1** and the increment in loss permittivity may be due to the extensive deposition of inorganic load on the surface of the polymeric matrix as infiltration time increases, indicating that smaller molecules are participating in the motion [8].

Figure 3 displays the Arrhenius plot for all relaxation spectra of the sSEBS and hybrid sSEBS, which shows a more detailed view of the modifications induced by infiltration of $40SiO_2$-$40P_2O_5$-$20ZrO_2$ inorganic filler. The β relaxation gives a linear dependence for the relaxation time τ, thus confirming its non-cooperative nature. However, the α_{EB} and α_{PS} processes show a nonlinear relationship between temperature and the relaxation times, characteristic of cooperative molecular motions. Therefore, the molecular motions will be analysed accordingly. The Arrhenius plot confirms the shift mentioned above toward lower frequencies of α_{PS}, which means a more significant plasticising effect caused by the formation of the inorganic network. However, prolonged infiltration does not necessarily observe the plasticising effect. For another thing, the α_{EB} displays a shift towards higher temperatures characteristic of crosslinked microstructures[36], but the increment of the infiltration time does not have a clear tendency. For instance, the most significant shift is found for the sSEBS-10 membrane. The membranes with 20 and 40 minutes of infiltration display a greater temperature than the sSEBS membrane, but the sSEBS-10 is bigger. Therefore, such behaviour could be ascribed to the existence of an optimum infiltration time, t_{inf} = 10 min. This time seems to display the right combination between the good values of electric permittivity and adequate cooperative motions of the PS block.

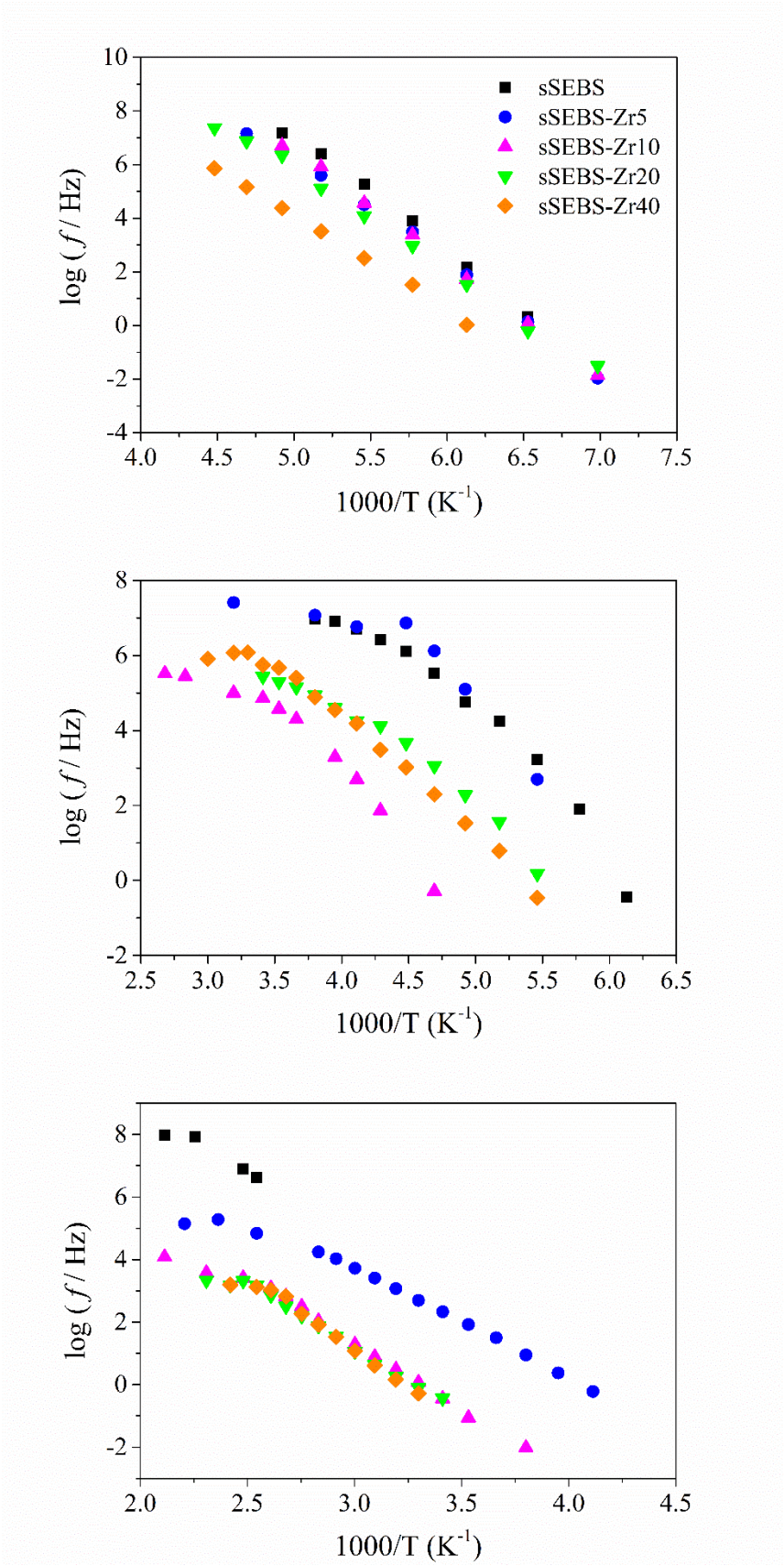

Figure 3. Arrhenius plot of the (top) β relaxation, (middle) α_{EB}, (bottom) α_{PS} found in the dielectric spectra of sulfonated SEBS (sSEBS) and all hybrid SEBS (sSEBS-Zr5, sSEBS-Zr10, sSEBS-Zr20 and sSEBS-Zr40).

3.1 The β dielectric relaxation

The β relaxation is a non-cooperative molecular motion that appears at low temperatures, more precisely, in the range of 166-184 K at a frequency of 1 kHz. Its origin is still unclear among researchers, as it has always been spotted in the mechanical spectrum but not in the dielectric one [6,44]. **Figure 4** exhibits the loss of dielectric permittivity at a frequency of 1 kHz of this β relaxation. It was observed that the maximum peak temperature of the sSEBS-Zr5, sSEBS-Zr10 and sSEBS-Zr20 β relaxations shift towards higher temperatures by the effect of the infiltration time. Still, this shift is more significant for the sSEBS-Zr40 relaxation peak.

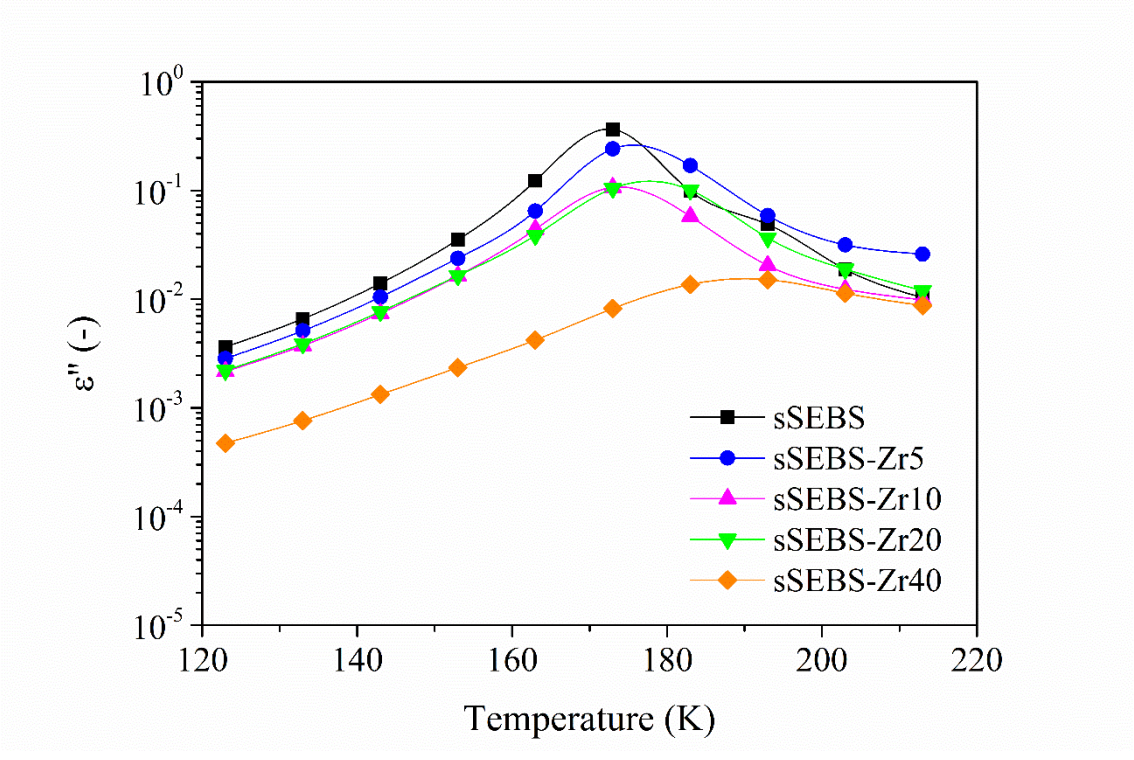

Figure 4. β relaxation for the sulfonated SEBS (sSEBS) and all hybrid SEBS (sSEBS-Zr5, sSEBS-Zr10, sSEBS-Zr20 and sSEBS-Zr40) at 1 kHz.

As expected, as the amount $40SiO_2$-$40P_2O_5$-$20ZrO_2$ filler increases, Si, Zr and P molecules increase; consequently, the resultant oxide network extends along the surface and across the thickness of the membranes as the infiltration time increases[8]. Thus, it takes more energy to excite the molecular motion, and subsequently, the entire relaxation process shifts towards higher temperatures.

Table 1 presents the apparent activation energy values E_a, which does have not a clear trend as a function of the infiltration time because they rise until 10 minutes and then decrease again.

Table 1. The apparent activation energy (E_a) at 1 Hz for SEBS, sSEBS and all hybrid sSEBS-Zr.

	Slope	**Intercept**	E_a **(kJ·mol^{-1})**	**R^2**
sSEBS	-4.15 ± 0.16	27.68 ± 0.88	72	0.991
sSEBS-Zr5	-3.87 ± 0.12	25.45 ± 0.67	74	0.992
sSEBS-Zr10	-4.21 ± 0.06	27.59 ± 0.35	81	0.999
sSEBS-Zr20	-3.71 ± 0.08	24.26 ± 0.47	71	0.996
sSEBS-Zr40	-3.50 ± 0.06	21.57 ± 0.32	67	0.998

To further assess the effect of the inorganic infiltration on the dielectric spectra, the values of the dielectric strength ($\Delta\varepsilon$) in combination with the Havriliak-Negami shape parameters (a and b) have been displayed in **Table 2**. The strength decreases as the infiltration time increases, i.e., a more increasingly extended inorganic network over time. More precisely, sSEBS-Zr10 and sSEBS-Zr20 show similar values. The sSEBS-Zr40 shows the lowest values due to a more extensive deposition of P, Si and Zr oxides net that insulates the membrane, effectively decreasing the conduction of electrons. Additionally, the values of the a and b parameters display generally a symmetric distribution for zero (sSEBS) or short infiltration times. On the contrary, there is a general tendency to move towards more asymmetric distributions at more significant infiltration times. Consequently, these results imply a diminishment in the number of molecules involved in the motion, which is an expected outcome considering that the electric conductivity diminishes with increasing infiltration time.

Table 2: Havriliak-Negami parameters for the β relaxation for the neat, sulfonated and hybrid SEBS.

	T (K)	Δε	a	b
sSEBS	163	0.93	0.88	0.72
	173	0.96	0.81	0.83
	183	1.30	0.76	0.65
	193	1.26	0.77	0.75
	203	1.12	0.83	0.71
sSEBS-Zr5	163	0.66	0.93	0.73
	173	0.64	0.93	0.69
	183	0.90	0.80	0.70
	193	0.89	0.80	0.72
	203	0.83	0.82	0.75
sSEBS-Zr10	163	0.32	0.82	0.56
	173	0.46	0.64	0.61
	183	0.44	0.71	0.49
	193	0.45	0.62	0.77
	203	0.41	0.66	0.82
sSEBS-Zr20	163	0.31	0.92	0.61
	173	0.27	0.92	0.62
	183	0.41	0.92	0.39
	193	0.43	0.89	0.40
	203	0.43	0.68	0.91
sSEBS-Zr40	163	0.09	0.60	0.52
	173	0.04	0.69	0.50
	183	0.07	0.68	0.29
	193	0.08	0.64	0.28
	203	0.09	0.61	0.29

3.2 The α_{EB} relaxation process.

Figure 5 displays the α_{EB} relaxation peak between 190 and 320 K at a frequency of 1 Hz. The presence of the $40SiO_2$-$40P_2O_5$-$20ZrO_2$ inorganic filler increases 30K after 5 minutes of infiltration time. However, after 10 minutes, the maximum temperature peak does not shift. The dynamic crosslinking created by the chemical bonds (M-OH, M-O-M with M = Si, P, Zr) hinders the mobility of the EB block, therefore, incrementing the temperature where the dielectric relaxation occurs.

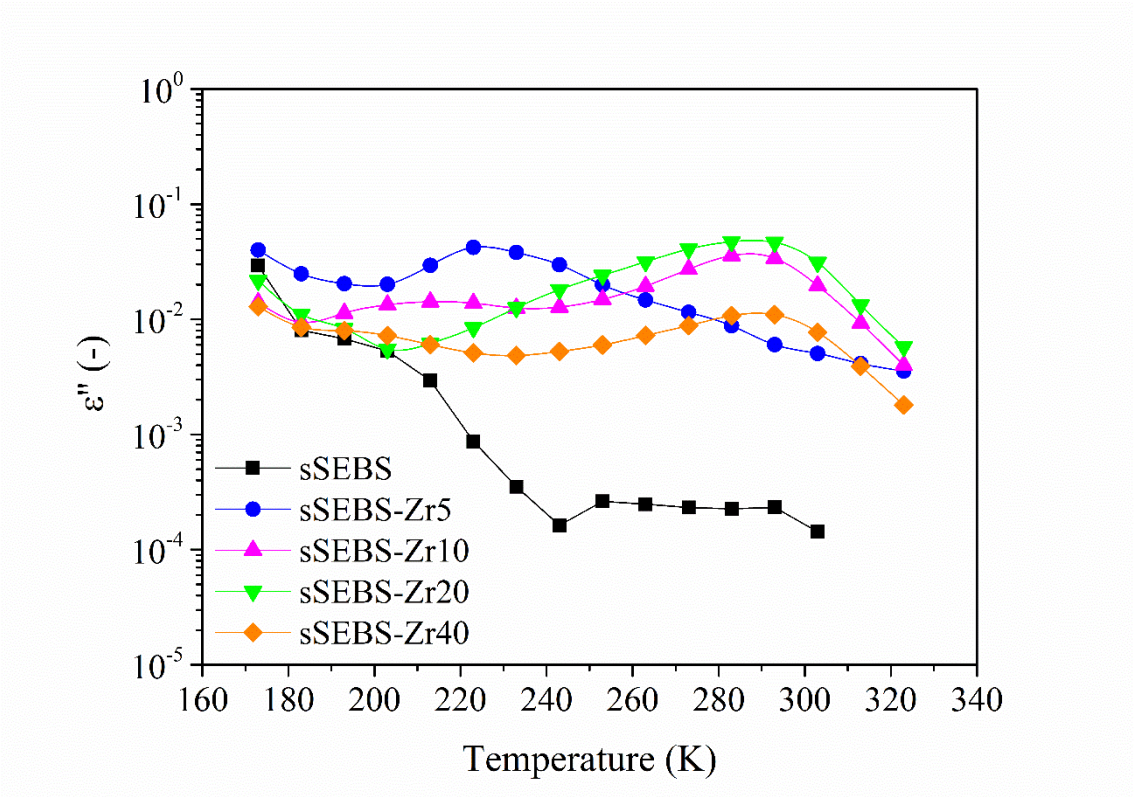

Figure 5. α_{EB} relaxation for the sulfonated SEBS (sSEBS) and all hybrid SEBS (sSEBS-5, sSEBS-10, sSEBS-20 and sSEBS-40) at 1 Hz.

The assessment of the temperature dependence of the dielectric strength ($\Delta\varepsilon$), displayed in **Table 3**, might help provide a more detailed view of the increment of the infiltration time to the relaxation process. Overall, the general trend is to diminish the strength of the process as the infiltration times increase.

Table 3. Parameters of the dielectric strength ($\Delta\varepsilon$) of the α_{EB} relaxation process for the neat, sulfonated and hybrid SEBS.

T (K)	sSEBS	sSEBS-Zr5	sSEBS-Zr10	sSEBS-Zr20	sSEBS-Zr40
213	0.24	0.36	0.13	0.01	0.07
223	0.17	0.41	0.11	0.05	0.03
243	0.11	0.44	0.13	0.03	0.06

The distribution of the inorganic filler on the surface and across the membrane generates a coating, which acts as an electric insulator. It is the case, for instance, of the sSEBS-Zr20 and sSEBS-Zr40, where fewer and fewer molecules can reorient with the applied

electric field. Subsequently, the strength of the dielectric relaxation decreases significantly.

Table 4. Fitting parameters for the VFTH model applied to the α_{EB} relaxation process for the sSEBS and the hybrid sSEBS-Zr. Derived parameters for the study of dynamic fragility.

Sample	VFTH				
	Log f₀	**B (K)**	**T_{VFTH} (K)**	**m**	**R^2**
sSEBS	9.79 ± 0.23	840.10 ± 69.60	127.36 ± 2.34	11	0.997
sSEBS-Zr5	8.48 ± 0.17	358.98 ± 48.45	156.25 ± 2.90	7	0.998
sSEBS-Zr10	7.51 ± 0.26	2559.87 ± 235.59	123.72 ± 8.51	5	0.996
sSEBS-Zr20	7.83 ± 0.19	874.95 ± 77.76	133.35 ± 3.39	6	0.998
sSEBS-Zr40	10.01 ± 1.34	1590.11 ± 92.56	122.88 ± 5.59	7	0.988

However, the hybrid membranes sSEBS-Zr show different tendencies when compared between them. The sSEBS-Zr5 has far larger values than the original sSEBS or the other hybrid membranes. This behaviour is explained because most of the inorganic network has located at the membrane's surface during a short infiltration time. Thus, these surface charges interact with the applied electric field, thus providing a stronger signal [45,46]. Furthermore, the sSEBS-Zr10 is the most regular, and the values are not that far from the ones displayed by the sSEBS membrane. Again, the infiltration time of 10 minutes seems to provide the best dielectric performance in conjunction with enhanced chemical and mechanical properties [8].

The temperature dependence of the α_{EB} molecular relaxation is calculated using the VFTH equation (**Eq.3**), and the analysis is performed in terms of fragility (**Eq.4**). The parameters for the best fit are gathered in **Table 4**. The fragility parameter provides valuable information about the molecular arrangement, which controls the microstructure of the membrane. For instance, it is immediately seen that sSEBS-Zr10 displays the lowest values of the fragility parameter and, accordingly, the strongest behaviour. This is in line with the low variability of the dielectric strength since polymers with lower fragility values can withstand sudden temperature changes, and their structure is not affected by them. This feature translates into a better membrane performance that might suffer temperature changes.

On the other hand, the other hybrid membranes also display low values of the fragility parameter, thus, a strong behaviour. Although it is not comparable to the one offered by sSEBS-Zr10, it is also very resistant to structural changes due to sudden temperature changes. In any case, the increment of the infiltration time provides a stronger behaviour thanks to the dynamic crosslinking.

3.3 The α_{PS} relaxation process.

The α_{PS} dielectric relaxation is a cooperative molecular motion that occurs at a temperature range from 375 K to 400 K at 1 kHz. **Figure 6** displays the complex part of the dielectric permittivity. Immediately, it can be observed that the hybrid membranes sSEBS-Zr present higher losses than the sSEBS. The losses increment with the infiltration time is characteristic of the dynamic crosslinking. However, the hybrid membranes sSEBS-Zr40 display the lowest permittivity of the hybrid sSEBS. This result would indicate that the infiltration time cannot be increased continuously to improve the electrical properties of these hybrid membranes, precisely due to the electrical insulating effect produced by the extensive deposition throughout the membrane.

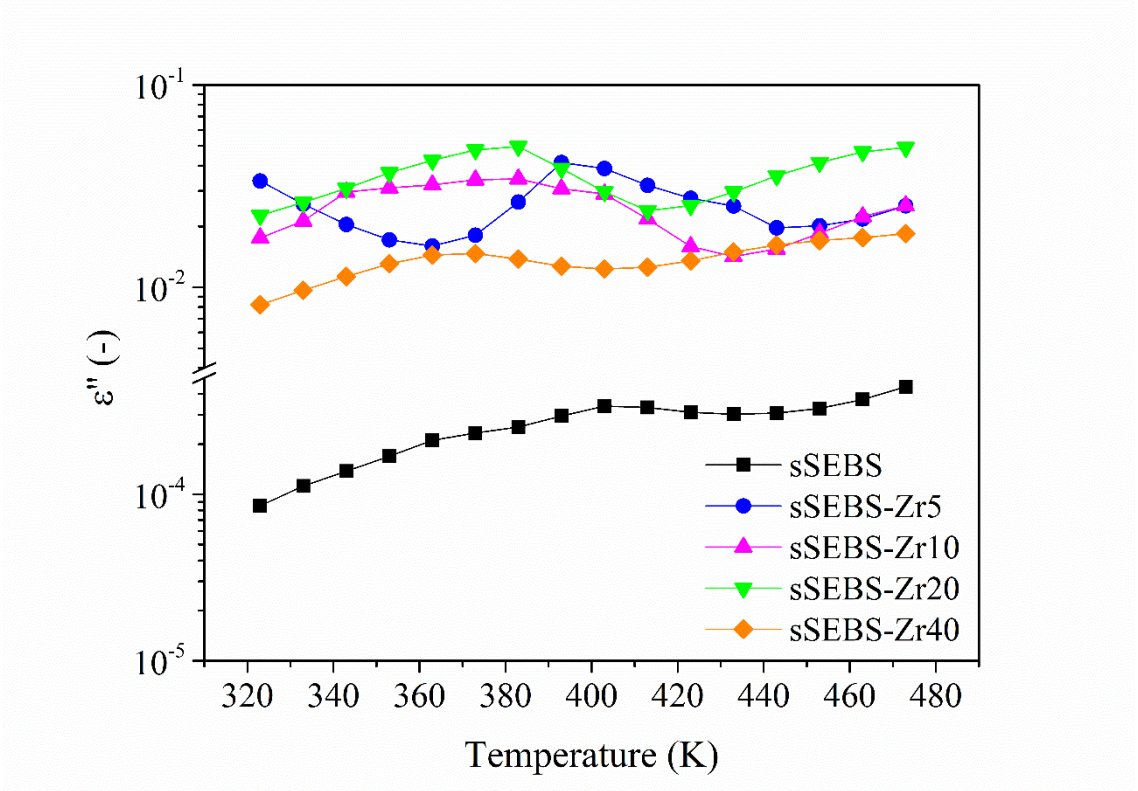

Figure 6. α_{PS} relaxation for the sulfonated SEBS (sSEBS) and all hybrid SEBS (sSEBS-Zr5, sSEBS-Zr10, sSEBS-Zr20 and sSEBS-Zr40) at 1kHz.

Additionally, the data presented in **Figure 6** shows a plasticisation effect, which agrees with the Arrhenius plot (**Figure 4**). Therefore, it can be concluded that the addition of the inorganic filler facilitates the molecular motions at high temperatures.

This plasticising effect causes a decrease in its temperature that gives rise to molecular motion related to the glass transition of the styrene phase. It occurs in the range of temperatures at which PEMFCs work. This result may indicate that at these temperatures, the mobility of the ions in the hybrid membranes sSEBS-Zr will be higher than in the only sulfonated membranes sSEBS. Likewise, as the motion of the glass transition is an intermolecular motion, the mobility of ions in this range of temperatures will be governed by a proton hopping (or Grotthuss mechanism) where the proton transfers through a hydrogen bond network and it is also considered to be more efficient.

Table 5. Parameters of the dielectric strength ($\Delta\varepsilon$) of the α_{PS} relaxation process for the neat, sulfonated and hybrid membranes.

T (K)	sSEBS	sSEBS-Zr5	sSEBS-Zr10	sSEBS-Zr20	sSEBS-Zr40
333	-	0.11	0.10	0.07	0.05
343	-	0.12	0.10	0.07	0.05
353	-	0.12	0.09	0.06	0.04

The analysis of the dielectric strength gathered in **Table 5** provides a clear view of adding the inorganic filler to this molecular relaxation process. Firstly, the plasticisation of the α_{PS} is evident because in the spectrum of sSEBS at this temperature range as no presence of this molecular motion. As in the other cooperative motion, the sSEBS-Zr5 displays larger values thanks to the heterogeneous distribution of the filler. As the infiltration time increases, the values of the dielectric strength diminish. It is expected since it has been shown that a large filler's concentration acts as an electric insulator.

Interestingly, the evolution of the dielectric strength as the temperature increases tends to achieve a slightly constant value and no sudden increases or drops occur. Additionally, no further variations are registered at higher temperatures. It can be concluded that at these low temperatures inside the operative range of a PEMFC, the entire backbone of the PS block is in a sweeping motion. Therefore, the filler effectively closes the gap between the two cooperative motions.

The temperature dependence of the relaxation times was assessed using the VFTH equation (**Eq.3**), and the results are gathered in **Table 6**.

Table 6. Best fitting parameters for the VFTH model applied to the α_{PS} relaxation process for the sulfonated and hybrid SEBS. Derived parameters for the study of the dynamic fragility.

Sample	VFTH				
	Log f_0	**B (K)**	**T_{VFTH} (K)**	**m**	**R^2**
sSEBS	14.89 ± 1.95	1306.05	213.12 ± 27.29	51	0.995
sSEBS-Zr5	8.31 ± 0.43	4594.06	107.16 ± 12.01	10	0.993
sSEBS-Zr10	7.33 ± 0.18	2115.3	166.71 ± 3.42	7	0.998
sSEBS-Zr20	8.01 ± 1.14	818.01	107.78 ± 35.96	16	0.988
sSEBS-Zr40	7.85 ± 1.19	3074.41	140.19 ± 32.52	15	0.991

The values gathered in **Table 6** show higher fragility parameter values for sSEBS membranes. Nonetheless, the addition of the inorganic filler brings the lowest and strongest behaviour, as the drop registered by the hybrid membranes is evidence. It agrees with the data presented in the Arrhenius plot (**Figure 3**) and reflects the same tendency observed for the α_{EB} dielectric relaxation.

However, there are no significant differences in the fragility value after infiltration times higher than 20 minutes. The main difference again is shown by the sSEBS-10 membrane, which possesses the strongest behaviour of them all, and therefore, it is less affected by the variations in the temperature range. Subsequently, considering that this molecular process is active when the membrane operates in real PEMFC conditions, it is now understood that it offers the best performance[8]. According to the data presented here, it will withstand better any temperature variation than any of the other membranes. Considering only this parameter, the optimum infiltration time is around 10-20 minutes since it provides acceptable values of electric permittivity and induces dynamic crosslinking to bring closer the glass transitions of both blocks.

These results agree with the previous results with the maximum power values obtained for a PEMFC, whose electrolyte is a hybrid sSEBS-Zr10 membrane[8] and validates the

384 proposed methodology. Therefore, a detailed analysis of the molecular mobility allows
385 fine-tuning the membranes for an optimum design focused on its application in a proton
386 exchange membrane fuel cell (PEMFC).

387

4. Conclusions

A series of hybrid sulfonated SEBS membranes infiltrated with $40SiO_2{-}40P_2O_5{-}20ZrO_2$ by sol-gel chemistry have been further investigated using dielectric thermal spectroscopy to evaluate their appropriateness for PEMFC applications. Accordingly, the spectra were composed of three dielectric relaxations, a non-cooperative (β) relaxation and two cooperative ($\alpha_{EB,}$ α_{PS}) ones ascribed to the glass transition of each block. The addition of the inorganic filler significantly impacts the cooperative motions.

The α_{EB} relaxation is hindered by the dynamic crosslinking formed by the polycondensation of M-O-M' bonds, and therefore, the dielectric relaxations are shifted towards higher temperatures. At higher temperatures, the α_{PS} displays a significant plasticisation effect which facilitates the chain motion, and subsequently, the relaxation processes are shifted towards lower frequencies and temperatures. Consequently, the spectra of the hybrid membranes are not characterised by a large gap between both cooperative motions as it occurs in the spectrum of both neat and sulfonated SEBS.

The analysis of the temperature dependence of the molecular relaxation reveals that the membrane with an infiltration time of 10 minutes has the strongest behaviour, resulting in a more thermally stable structure. Accordingly, considering that the two cooperative motions are active during the operating range of a PEMFC, this membrane will adapt better to any temperature variation without compromising its performance significantly.

Therefore, an infiltration time of 10 minutes is the optimum since it displays the right combination of the following factors: good values of electric permittivity, a dynamic crosslinking that shifts the α_{EB} towards higher temperatures and the easing of the α_{PS} relaxation to move this molecular process towards lower temperatures near to the range of temperatures at which PEMFCs work.

Accordingly, a comprehensive characterisation of the molecular mobility provides enough information to properly design membranes for an optimum composition to be useful as polyelectrolytes in PEMFCs.

5. Acknowledgments

The authors would like to thank the support of the European Union through the European Regional Development Funds (ERDF) and the Spanish Ministry of Economy, Industry and Competitiveness for the research POLYELMETH (PID2020-116322RB-C31).

6. References

[1] M. Casciola, A. Donnadio, M. Pica, 3.7 Basic Aspects in Proton-Conducting Membranes for Fuel Cells, in: Compr. Membr. Sci. Eng., Elsevier Ltd., 2017: pp. 171–205. https://doi.org/10.1016/b978-0-12-409547-2.12259-0.

[2] Y.A. Elabd, M.A. Hickner, Block copolymers for fuel cells, Macromolecules. 44 (2011) 1–11. https://doi.org/10.1021/ma101247c.

[3] J. Meier-Haack, A. Taeger, C. Vogel, K. Schlenstedt, W. Lenk, D. Lehmann, Membranes from sulfonated block copolymers for use in fuel cells, Sep. Purif. Technol. 41 (2005) 207–220. https://doi.org/10.1016/j.seppur.2004.07.018.

[4] C. Del Río, O. García, E. Morales, P.G. Escribano, Single cell performance and electrochemical characterization of photocrosslinked and post-sulfonated SEBS-DVB membranes, Electrochim. Acta. 176 (2015) 378–387. https://doi.org/10.1016/j.electacta.2015.07.009.

[5] C.A. Edmondson, J.J. Fontanella, S.H. Chung, S.G. Greenbaum, G.E. Wnek, Complex impedance studies of S-SEBS block polymer proton-conducting membranes, Electrochim. Acta. 46 (2001) 1623–1628. https://doi.org/10.1016/S0013-4686(00)00762-3.

[6] R. Teruel-Juanes, B. Pascual-Jose, C. del Río, O. García, A. Ribes-Greus, Dielectric analysis of photocrosslinked and post-sulfonated styrene-ethylene-butylene-styrene block copolymer based membranes, React. Funct. Polym. 155 (2020) 104715. https://doi.org/10.1016/j.reactfunctpolym.2020.104715.

[7] R.S. Raja Rafidah, W. Rashmi, M. Khalid, W.Y. Wong, J. Priyanka, Recent progress in the development of aromatic polymer-based proton exchange membranes for fuel cell applications, Polymers (Basel). 12 (2020). https://doi.org/10.3390/POLYM12051061.

[8] P.G. Escribano, C. del Río, E. Morales, M. Aparicio, J. Mosa, Infiltration of 40SiO2−40P2O5−20ZrO2 sol-gel in sSEBS membranes for PEMFCs application, J. Memb. Sci. 551 (2018) 136–144. https://doi.org/10.1016/j.memsci.2018.01.044.

[9] C.Y. Wong, W.Y. Wong, K. Ramya, M. Khalid, K.S. Loh, W.R.W. Daud, K.L. Lim, R. Walvekar, A.A.H. Kadhum, Additives in proton exchange membranes for low- and high-temperature fuel cell applications: A review, Int. J. Hydrogen Energy. 44 (2019) 6116–6135. https://doi.org/10.1016/j.ijhydene.2019.01.084.

[10] Y. Wang, D.F. Ruiz Diaz, K.S. Chen, Z. Wang, X.C. Adroher, Materials, technological status, and fundamentals of PEM fuel cells – A review, Mater. Today. 32 (2020) 178–203. https://doi.org/10.1016/j.mattod.2019.06.005.

[11] Y. Akinay, I. Nuri, Synthesis and characterization of the pearlescent pigments based on mica deposited with SiO 2 , AlN and TiO 2 : First report of its dielectric properties, Ceram. Int. (2020) 0–1. https://doi.org/10.1016/j.ceramint.2020.04.078.

[12] P. Basak, S. V. Manorama, R.K. Singh, O. Parkash, Investigations on the mechanisms of ionic conductivity in PEO-PU/PAN semi-interpenetrating polymer network-salt complex polymer electrolytes: An impedance spectroscopy study, J. Phys. Chem. B. 109 (2005) 1174–1182. https://doi.org/10.1021/jp0460792.

[13] T. Dam, S.N. Tripathy, M. Paluch, S.S. Jena, D.K. Pradhan, Investigations of Relaxation Dynamics and Observation of Nearly Constant Loss Phenomena in PEO20-LiCF3SO3-ZrO2 Based Polymer Nano-Composite Electrolyte, Electrochim. Acta. 202 (2016) 147–156. https://doi.org/10.1016/j.electacta.2016.03.134.

[14] H. Junoh, J. Jaafar, N.A.H. Nik Abdul, A.F. Ismail, M.H.D. Othman, M.A. Rahman, F. Aziz, N. Yusof, Performance of polymer electrolyte membrane for direct methanol fuel cell application: Perspective on morphological structure, Membranes (Basel). 10 (2020). https://doi.org/10.3390/membranes10030034.

[15] S. Kango, S. Kalia, A. Celli, J. Njuguna, Y. Habibi, R. Kumar, Surface modification of inorganic nanoparticles for development of organic-inorganic nanocomposites - A review, Prog. Polym. Sci. 38 (2013) 1232–1261.

https://doi.org/10.1016/j.progpolymsci.2013.02.003.

[16] M.C. Rao, R. Koutavarapu, K.V. Kumar, Structural and electrochemical properties of ZrO2 doped PVP-Na+ based nanocomposite polymer films, Mater. Sci. Semicond. Process. 89 (2019) 41–50. https://doi.org/10.1016/j.mssp.2018.08.030.

[17] A. Sivasankaran, D. Sangeetha, Y.H. Ahn, Nanocomposite membranes based on sulfonated polystyrene ethylene butylene polystyrene (SSEBS) and sulfonated SiO2 for microbial fuel cell application, Chem. Eng. J. 289 (2016) 442–451. https://doi.org/10.1016/j.cej.2015.12.095.

[18] S. Zulfiqar, Z. Ahmad, M. Ishaq, S. Saeed, M.I. Sarwar, Thermal and mechanical properties of SEBS-g-MA based inorganic composite materials, J. Mater. Sci. 42 (2007) 93–100. https://doi.org/10.1007/s10853-006-1082-8.

[19] H.A. Bolados, M. Hernández-Santana, L.J. Romasanta, M. Yazdani-Pedram, R. Quijada, M.A. López-Manchado, R. Verdejo, Electro-mechanical actuation performance of SEBS/PU blends, Polymer (Guildf). 171 (2019) 25–33. https://doi.org/10.1016/j.polymer.2019.03.035.

[20] Z.-M. Dang, J.-K. Yuan, J.-W. Zha, P.-H. Hu, D.-R. Wang, Z.-Y. Cheng, High-permittivity polymer nanocomposites: Influence of interface on dielectric properties, J. Adv. Dielectr. 03 (2013) 1330004. https://doi.org/10.1142/s2010135x13300041.

[21] V. Di Noto, S. Lavina, E. Negro, M. Vittadello, F. Conti, M. Piga, G. Pace, Hybrid inorganic-organic proton conducting membranes based on Nafion and 5 wt% of MxOy (M = Ti, Zr, Hf, Ta and W). Part II: Relaxation phenomena and conductivity mechanism, J. Power Sources. 187 (2009) 57–66. https://doi.org/10.1016/j.jpowsour.2008.10.066.

[22] L. Dos Santos, O. Dubrunfaut, J.C. Badot, C. Laberty-Robert, Interplay between Electrical Relaxation and Structural Properties in Hybrid Membrane Based on PVDF-HFP and Functionalized Silica Network, J. Phys. Chem. C. 120 (2016) 6963–6970. https://doi.org/10.1021/acs.jpcc.6b00053.

[23] S.D. Mikhailenko, F. Celso, M.A.S. Rodrigues, S. Kaliaguine, Dielectric Measurements of Polymer Electrolyte Based Composites as a Technique for

509 Evaluation of Membrane Homogeneity, Electrochim. Acta. 136 (2014) 457–465.
510 https://doi.org/10.1016/j.electacta.2014.05.040.

511 [24] G. Nawn, K. Vezzù, F. Bertasi, G. Pagot, G. Pace, F. Conti, E. Negro, V. Di
512 Noto, Electric response and conductivity mechanism reciprocity in H3PO4-doped
513 Polybenzimidazole-4N-ZrO2 nanocomposite membranes, Solid State Ionics. 320
514 (2018) 172–176. https://doi.org/10.1016/j.ssi.2018.03.003.

515 [25] B. Sannakki, A. Anita, Dielectric properties of PMMA and its composites with
516 ZrO2, Phys. Procedia. 49 (2013) 15–26.
517 https://doi.org/10.1016/j.phpro.2013.10.006.

518 [26] J. Zhou, Y. Jiang, G. Wu, W. Wu, Y. Wang, K. Wu, Y. Cheng, Investigation of
519 dielectric and thermal conductive properties of epoxy resins modified by core-
520 shell structured PS@SiO2, Compos. Part A Appl. Sci. Manuf. 97 (2017) 76–82.
521 https://doi.org/10.1016/j.compositesa.2017.03.005.

522 [27] I.A. Stenina, A.B. Yaroslavtsev, Ionic mobility in ion-exchange membranes,
523 Membranes (Basel). 11 (2021). https://doi.org/10.3390/membranes11030198.

524 [28] C. González-Guisasola, A. Ribes-Greus, Dielectric relaxations and conductivity
525 of cross-linked PVA/SSA/GO composite membranes for fuel cells, Polym. Test.
526 67 (2018) 55–67.

527 [29] A.R. Young-Gonzales, S.J. Paddison, A.P. Sokolov, Tuning proton conductivity
528 and energy barriers for proton transfer, J. Chem. Phys. 154 (2021).
529 https://doi.org/10.1063/5.0032512.

530 [30] S. Havriliak, S. Negami, A complex plane representation of dielectric and
531 mechanical relaxation processes in some polymers, Polymer (Guildf). 8 (1967)
532 161–210. https://doi.org/10.1016/0032-3861(67)90021-3.

533 [31] S. Havriliak, S. Negami, A complex plane analysis of α-dispersions in some
534 polymer systems, J. Polym. Sci. Part C Polym. Symp. 14 (1966) 99–117.
535 https://doi.org/10.1002/polc.5070140111.

536 [32] J.M. Charlesworth, Deconvolution of overlapping relaxations in dynamic
537 mechanical spectra, J. Mater. Sci. 28 (1993) 399–404.
538 https://doi.org/10.1007/BF00357816.

539 [33] H. Vogel, The law of the relation between the viscosity of liquids and the

temperature, Phys. Z. 22 (1921) 645–646.

[34] H. Vogel, Über die Dissociationswärme und den Einfluss der Temperatur auf den Dissociationsgrad der Elektrolyte, Zeitschrift Für Phys. Chemie. 4U (1889) 96. https://doi.org/10.1515/zpch-1889-0408.

[35] G. Tammann, W. Hesse, Die Abhängigkeit der Viscosität von der Temperatur bie unterkühlten Flüssigkeiten, Zeitschrift Für Anorg. Und Allg. Chemie. 156 (n.d.) 245–257. https://doi.org/10.1002/zaac.19261560121.

[36] E. Riande, R. Díaz-Calleja, Electrical properties of polymers, CRC Press, 2004.

[37] W. Kauzmann, Dielectric Relaxation as a Chemical Rate Process, Rev. Moden Phys. 14 (1942) 12–44.

[38] W. Kauzmann, The Nature of the Glassy State and the Behavior of Liquids at Low Temperatures, Chem. Rev. 43 (1948) 219–256. https://doi.org/10.1021/cr60135a002.

[39] J. Heijboer, Molecular origin of relaxations in polymers, Ann. N. Y. Acad. Sci. 279 (1976) 104–116. https://doi.org/10.1111/j.1749-6632.1976.tb39700.x.

[40] H. Eyring, The activated complex in chemical reactions, J. Chem. Phys. 3 (1935) 107–115. https://doi.org/https://doi.org/10.1063/1.1749604.

[41] G.S. Fulcher, Analysis of recent measurements of the viscosity of glasses, J. Am. Ceram. Soc. 8 (n.d.) 339–355. https://doi.org/10.1111/j.1151-2916.1925.tb16731.x.

[42] A.K. Doolittle, Studies in Newtonian Flow. II. The Dependence of the Viscosity of Liquids on Free-Space, J. Appl. Phys. 22 (1951) 1471. https://doi.org/10.1063/1.1699894.

[43] A.K. Doolittle, Studies in Newtonian Flow. III. The Dependence of the Viscosity of Liquids on Molecular Weight and Free Space (in Homologous Series), J. Appl. Phys. 23 (1952) 236. https://doi.org/10.1063/1.1702182.

[44] H. Chen, M.K. Hassan, S.K. Peddini, K.A. Mauritz, Macromolecular dynamics of sulfonated poly (styrene-b-ethylene-ran-butylene-b-styrene) block copolymers by broadband dielectric spectroscopy, Eur. Polym. J. 47 (2011) 1936–1948. https://doi.org/10.1016/j.eurpolymj.2011.07.005.

[45] C. Gainaru, E.W. Stacy, V. Bocharova, M. Gobet, A.P. Holt, T. Saito, S. Greenbaum, A.P. Sokolov, Mechanism of Conductivity Relaxation in Liquid and Polymeric Electrolytes: Direct Link between Conductivity and Diffusivity, J. Phys. Chem. B. 120 (2016) 11074–11083. https://doi.org/10.1021/acs.jpcb.6b08567.

[46] A. Kisliuk, V. Bocharova, I. Popov, C. Gainaru, A.P. Sokolov, Fundamental parameters governing ion conductivity in polymer electrolytes, Electrochim. Acta. 299 (2019) 191–196. https://doi.org/10.1016/j.electacta.2018.12.143.